COOLANT VOID REACTIVITY IN A CANDU: A 2–D TRANSPORT/DIFFUSION COMPARISON

G. Marleau and E. Varin
Institut de génie nucléaire, École Polytechnique de Montréal
C.P. 6079, succ. Centre-ville, Montréal, Québec H3C 3A7
guy.marleau@polymtl.ca; elisabeth.varin@polymtl.ca

ABSTRACT

We have analyzed using diffusion and transport theory methods an axially infinite 2–D representation of a CANDU reactor fueled with 37 element bundles. Our studies indicate that a relatively fine mesh is required to ensure that the reactor model is spatially converged for both diffusion and transport calculations. The effect of using the more physical annular boundary condition in transport is very small while it leads to much higher errors in diffusion.

The power distribution computed using diffusion theory are more peaked towards the core center than their transport counterpart with differences reaching 6 % near the core/reflector interface. When full cell homogenization is considered, the differences in the coolant void reactivity between a transport and a diffusion calculation show that the diffusion theory simulates relatively well this effect. On the other hand, using the pin model in transport yields much larger differences in coolant void reactivity.

I. INTRODUCTION

Most CANDU reactor simulations are realized in diffusion theory because it is believed that this approximation is adequate to represent the neutron behavior inside the core. A 3–D Cartesian model is generally considered and computer codes such as RFSP[3] or DONJON[4] are used to evaluate the power distribution inside the core. Fuel cell properties depending on the burnup are obtained from transport calculations using codes such as WIMS-AECL[1] or DRAGON.[2] Those properties are generally condensed to a 2 energy group structure for cooled and voided configurations. The properties could then be incorporated in a time-average model of the reactor designed to reproduce an equilibrium state of the core or in any other burnup distribution representative of the reactor at the time of the voiding. The coolant void reactivity (CVR) is finally calculated in static theory from the two eigenvalues computed for the voided and cooled reactor configurations.

The diffusion approximation implies that the boundary conditions must be approximated by zero flux conditions on an extrapolated boundary. Moreover, the validity of Fick's law can

be questioned at the core reflector interface where large changes in physical properties are observed. These two approximations could lead to large flux differences in the reflector and in the last radial fuel regions, thereby affecting the precision of the computed bundle powers and CVR.

The solution to the transport equation will be obtained using the collision probability (CP) based transport code DRAGON. Here the main approximation consists in assuming that the source inside each region of the calculation mesh is flat. This means that a fine mesh discretization is required to ensure that a reliable transport solution is obtained. As a result, the amount of memory necessary to analyze the full 3–D reactor is considerable. We therefore propose to use an axially infinite 2–D model for the reactor.

The simplified 2–D representation of the reactor will be presented and studied in the context of diffusion and transport calculations. Here we have validated the diffusion approximations using the transport equation on a reactor model. A comparison between the transport and diffusion power distributions quantifies the errors that can be associated with diffusion theory. Both cooled and fully voided representation of the core have been considered. The effect of different models and calculation approximations on the CVR have also been studied.

II. MODELS

II.A. Cell Models

Before discussing in details the 2–D reactor models considered in this analysis, it is important to discuss first the generation of the cell properties required in our calculations. Here the standard 37 element CANDU-6 fuel cell was considered. The burnup dependent cross sections required for our reactor calculations were generated using the DRAGON code where we assumed that the fuel depletes at a fixed power density of 31.97 kW/kg during 300 days with time steps of 1 day.

At each time step, the DRAGON computed multi-group and multi-region flux distribution are used to evaluate 2-group homogenized cross sections. Here two different cell homogenization procedures are considered. First, we performed a full cell homogenization following the standard procedure for CANDU reactor calculations. We also decided to generate separately the properties of the fuel, the pressure to calandria tubes and the moderator. These properties were generated in DRAGON using the SPH homogenization procedure that ensures that the 3 region homogenized properties are totally coherent with the homogeneous fuel cell properties generated using the standard flux/volume homogenization method.[5]

II.B. Time-Average Models

The cell-average properties are then used for a 3–D reactor calculation in diffusion theory using the code DONJON. The goal of this calculation is to obtain a time-average burnup distribution in the core that can be used in our 2–D reactor model. Here we considered a coarse mesh ($26 \times 26 \times 12$) 3–D reactor model without reactivity control devices. Two combustion zones are then defined and an average exit burnup is computed in such a way as to maintain a

super-critical core with $k_{eff} = 1.020$. This should account for the absence of the absorber rods (15 mk) and liquid zone controllers (5 mk) in our 3–D core model.

A channel age pattern is then considered to determine the specific burnup of each fuel bundle based on the resulting time-average burnup distribution.[6] To obtain a 2–D burnup distribution, the 4560 values are averaged with respect to the bundle powers using:

$$B_j = \frac{\sum_i B_{ij} P_{ij}}{\sum_i P_{ij}} \quad \text{for} \quad j = 1, 380 \tag{1}$$

The burnup distribution is transformed into a depletion time pattern, each time step being rounded of to an integer number of days. This rounding off is convenient because it avoids interpolation in the fuel tables (the cross sections tables were tabulated with time steps of 1 day). Since DRAGON does not have cross sections interpolation capability, this procedure guarantees that the DRAGON transport and DONJON diffusion calculations will be performed using exactly the same 2-group cross section library.

II.C. 2–D Diffusion Models

Our 2–D model, illustrated in Figure 1, represents a mid-plane cut of a CANDU–6 at the location of maximal reflector width. It is defined by a Cartesian mesh in which virtual cells (empty boxes) represent the regions outside the annular boundary. At first, we chose the same Cartesian mesh as that used for the follow-up and analysis of Gentilly-2.[7] The reflector shield is divided into 4 regions along the x and y axes. The fuel cells are also divided into 2 sub-regions along the x direction around the control rod locations in order to be able to apply incremental cross sections to the half-cells these rods will affect. There is no mesh splitting in the y direction for the fuel cells. This then yields a 44×30 region model. The properties of each fuel cell in the reactor, which are homogenized over one lattice pitch, depend on fuel burnup. The reflector properties are assumed burnup independent. Cylindrical boundary conditions are applied on the last reflector cells at the annular boundary.[8]

For all of our analysis we have used a mesh description which is more refined than that found in the reference geometry. In fact, each fuel cell has been subdivided into 2 sub-regions in each direction x and y. The reflector shield is also divided into 5 meshes, 4 of which are half a lattice pitch wide while the last mesh is 11.375 cm wide. The final model then contains 54×54 regions of approximately the same volume. This model has the advantage that in the case where all the fuel cells have the same burnup, the resulting flux will be symmetric in both the x and y directions.

Now, in order to obtain the neutron flux distribution inside the reactor, the boundary conditions used in diffusion theory must simulate as well as possible zero re-entrant flux conditions on the annular boundary. In diffusion theory, this condition is approximated using:

$$\phi(x) + 2D\frac{d\phi}{dx} = 0 \tag{2}$$

In diffusion codes, this approximate boundary condition can be simulated in several ways. One can show that this is equivalent to a zero flux ($\phi(x) = 0$) boundary condition at an extrapolated

distance $R + \delta r(E)$ where R is the core radius and $\delta r(E)$ an energy dependent extrapolation distance. One can first assume that the flux vanishes at the interface between the reflector and the virtual cells ($\delta r(E) = 0$), this is called the "ZERO" flux boundary condition. A second option consists in assuming that the flux vanishes at an extrapolated distances $x + \delta r(E)$ and/or $y + \delta r(E)$ inside the virtual cells. This option is called the "VOID" flux boundary condition. Finally, one can use angle dependent extrapolation distances $\delta x(\theta, E)$ and $\delta y(\theta, E)$ (here θ is the cell angular location), called the cylindrical boundary condition.[8]

Our second concern is associated with the validity of the diffusion approximation at the fuel-reflector boundary. In the case where an infinite array of fuel is considered, one expect the flux variations inside the core to be small since the cell cross sections vary weakly as a function of fuel burnup. On the other hand, the cross section associated with the reflector are very different from those associated with the fuel cell and large flux variations are expected in regions close to the fuel/reflector interface. To study this effect, our 2–D base model of 54×54 Cartesian cells will be subdivided using a uniform n fold mesh splitting in both the x and y directions. Since the number of regions that can be considered in our transport calculations is limited, we decided to use only symmetric $1/4$ and $1/8$ core models where the burnup distributions were those found in the upper right corner of the reference core (see Figure 1).

II.D. 2–D Transport Models

Here three models are considered. The first model is similar to the 2–D CANDU model used for the diffusion calculation. Here, the virtual cells are replaced by voided cells. In this case the properties of each fuel cell in the reactor are homogenized over one lattice pitch and depend on fuel burnup while the reflector properties are burnup independent. The void boundary conditions are applied at the Cartesian cell limits and are identical to zero re-entrant flux at the reflector/void interface. The second model is similar to the first model with the exception that the annular reflector boundary is explicitly simulated as illustrated in Figure 2.

Finally, the pin model presented in Figure 3 is also considered. In this case, each fuel cell is subdivided into 3 sub-regions that consists in an annular fuel/coolant region surrounded by an annular pressure-calandria tube region inside a Cartesian moderator. The properties of each fuel cell in the reactor, which are homogenized over 3 regions depend again on fuel burnup while the reflector properties are burnup independent. Using this model, one should be able to evaluate the errors in the power distribution inside the core due to the full cell homogenization. In addition, this model should be less sensitive to the spatial discretization at the interface between the fuel and reflector region because the properties of the reflector are similar to those of the cell moderator region.

III. DIFFUSION-DIFFUSION ANALYSES

III.A. Calculation Methodology

The diffusion equation will be solved using the DONJON code. The mesh centered finite difference (MCFD) method implemented in the TRIVAC module is used for most of our

analysis.[9] However, for verification purpose, the effect of higher order finite difference methods has also been studied. Finally a symmetric $1/4$ core burnup distribution has been considered in all of our calculations.

In order to compare the results, fluxes and powers are normalized to a total thermal power of 2061.4 kW. To compare different mesh splitting, a flux homogenization is also realized on a coarse 30×30 regions mesh, where each region is one lattice pitch wide. Void effect is studied for a full voiding of the core.

III.B. Spatial Effects

First we analyze the effect of different boundary conditions using our 54×54 model, with a 1/4 core symmetric burnup distribution. We observe differences of up to 30% at the external boundary for the fast flux and up to 40% for the thermal flux when "VOID" are compared with cylindrical conditions. At the core/reflector interface, these differences reach 5% for the fast and 2% for the thermal fluxes. The fluxes differences inside the fuel regions remain within the 1% margin. These large differences have an overall effect of underestimating the powers by nearly 4% in the peripheral region. When compared with "ZERO" conditions (demonstrated to be less adequate than "VOID" conditions),[10] these flux and power differences have the same overall pattern but the power decrease can now reach 5% at the periphery of the core. Figure 4 shows the power distribution in a quarter of the core for the 54×54 model and the relative differences in power between "ZERO" and cylindrical boundary conditions. The powers are given in tens of kW and the differences are in %.

Another way of improving the diffusion solution at the core/reflector interface consists in refining the model. The original 54×54 model is split by 2,3,4 and 5 in each direction. Comparisons have been made for every boundary condition with respect to the very fine 270×270 mesh. In the case of "ZERO" boundary conditions, one observes that the flux spatial convergence is reached for a split 3 in each direction. However, the 4 % power differences with respect to the cylindrical conditions remain. In case of "VOID" boundary conditions, the differences in power distributions indicate that the spatial convergence is reached from split 3, but the power errors from the cylindrical boundary conditions stay at the 2% level at the core periphery. The mesh splitting seems to have more effect on fast than on thermal flux.

Finally the model with cylindrical conditions was also refined using split levels of 2 and 3 in each direction. The flux differences between the split 2 and 3 are under a few % and spatial convergence seems to be reached. The power differences between the coarse model and a 2×2 splitting are shown in Figure 5. Differences of up to 3% are observed at the core/reflector interface. This is expected because when a cell is divided into 4 sub-cells the boundary conditions are now applied independently on twice as many external surfaces.

Finally the TRIVAC solver provides high order finite difference methods that can be used to improve our solution.[11] Those methods, which are based on nodal collocation, have been chosen for the first order (equivalent to mesh centered finite differences), then for quadratic, cubic and quartic nodal collocations, in the case of "VOID" boundary conditions since the cylindrical correction was not implemented for high order finite difference methods. Fast flux in the reflector is up to 30% larger in the low order approach (MCFD 1) than in the highest

approach (MCFD 4), whereas thermal flux differences are under 10% in the reflector. In the fuel region, the flux differences are within 4%. The corresponding power differences are mainly located in the outer ring and remains under 2%. These differences are compatible to those obtained with our mesh splitting effort since the two approaches are comparable. One then has the choice of using a finer model or a higher order finite difference method.

From these comparisons one can say that the cylindrical boundary conditions contribute to a power increase in the outer ring of the reactor compared to other boundary conditions. For such boundary conditions, refinement effort re-enforces this tendency, as shown in Figure 5. We then choose the 104×104 mesh model with cylindrical boundary conditions as the reference when comparing with the transport results.

III.C. Void Effect

Even if all of these models show considerable differences in fluxes and power distributions in the core, their eigenvalues are very similar, even identical. Boundary conditions or mesh splitting have almost no effect on eigenvalues either for cooled or voided case. The eigenvalue of the cooled reactor is $k_{\mathit{eff}} = 1.03415$ while the eigenvalue of the voided case is $k_{\mathit{eff}} = 1.04906$ for the converged model. The coolant void reactivity, which is computed using

$$\rho = 1000 \left(\frac{k_{\mathit{eff}}^{Voided} - k_{\mathit{eff}}^{Cooled}}{k_{\mathit{eff}}^{Voided} k_{\mathit{eff}}^{Cooled}} \right) \tag{3}$$

is $\rho = 13.7$ mk.

For the different core configurations used in the previous section, voided calculations were also performed. The fluxes and powers are normalized to the same level for both the cooled and voided calculations. When the core is totally voided, the fast fluxes increase by about 4% at the center of the core and by up to 7% at the core/reflector interface. The thermal fluxes decrease in the core center by nearly 5% and by less than 2% in the reflector region. The power differences show an increase in the outer ring and almost no effects in the core center. The coolant voiding has no significant effect on the flux shape inside the fuel regions. The flux in the reflector increases as the neutron streaming outside the core region increase due to the lack of absorption in the coolant. The diffusion model developed here seems appropriate to follow those effects.

IV. TRANSPORT-TRANSPORT ANALYSES

IV.A. Calculation Methodology

The transport equation will be solved using the lattice code DRAGON. The CP option of DRAGON was selected even if a 2–D characteristic option is also available to perform such calculations. The main approximation that affects the precision of the results in both the CP and characteristics method is the requirement that the source must be flat inside each region of the calculation mesh considered.

For full reactor calculations (zero re-entrant flux conditions), the precision of DRAGON is only controlled by the size of the spatial calculation mesh considered. In lattice cell calculations the mesh is generally selected in such a way that it is smaller than the neutron mean free path inside each region. For our 2–D reactor model this implies a 2–D mesh size of about 1 cm^2 and consequently around 600K individual regions in the model. The amount of memory that is required to execute DRAGON on such a large problem is around 9 Tbytes. This is clearly out of reach for current computer systems. With our computers, the amount of memory available is around 1 Gbytes corresponding to a problem involving 7000 unknowns per group. Since our study cannot be completed for the full reactor model, we have considered instead a simplified model corresponding to 1/4 or about 1/8 of the original model (note that the 1/8 model contains only 376 fuel cell as can be seen in Figure 1).

For our 2–D reactor model, the cross section variations from fuel region to fuel region are relatively weak and, in principle, a coarse mesh model can be selected. The main errors then arise because of the presence of the reflector and even more importantly of the void region. Since there are no re-entering flux at the reflector/void interface, one expects the neutron flux distribution in the reflector region to decrease rapidly as the distance from the center of the core increases. As a result the diffusion sources in the reflector region are not flat. This should have a large effect on the flux distribution in the fuel cells located near the reflector zone. Accordingly, one should consider a fine radial mesh for the reflector zone as well as for the fuel region at the core periphery.

IV.B. Spatial Effects

In order to study the spatial convergence of the transport solution, a series of transport calculations with different spatial meshes was performed. The 1/8 core 27×27 region model was subdivided into $n = 2, 3$ and 4 equal meshes in both the x and y directions resulting in an increase for the number of regions by factors of 4, 9 and 16 respectively. For the finer model ($n = 4$) this lead to a 2–D mesh size of 3.57×3.57 cm^2 which can be compared with the original mesh ($n = 1$) of 14.3×14.3 cm^2.

Assuming that the reference solution is provided when the finer mesh ($n = 4$) is used, the relative error in the fluxes can be computed. The results are presented in Figure 6. As one can see, for $n = 3$ the maximum difference in the integrated flux inside the fuel zone is 1.2 % while in the reflector this error can reach 7.1 %. The error in the flux for the void zone past the reflector is somewhat larger since it can reach 18 % in the upper half corner of the core. Typically, this means that for the simple Cartesian description of the reactor, one can expect uncertainties in the computed power distribution errors of about 1% for the $n = 3$ model while for $n = 2$ and $n = 1$ the uncertainties will reach 2.5 % and 6.1 % respectively. The spatial convergence of the thermal flux along the x axis (see Figure 1) as a function of n can also be observed in Figure 7. The results with $n = 1$ show large errors both at the core center and at the fuel/reflector interface. On the other hand, convergence is clearly reached for $n = 3$.

We also compared the results obtained using the pin model with those obtained with the Cartesian model with a fine mesh ($n = 4$). Here we observe that the maximum differences in power distribution inside the fuel region is about 3.0 % for a coarse mesh model while for

$n = 2$ this error is reduced to 1.5 %. This shows that both the pin and the homogenized cell models converge to the same answer. Moreover, as expected from the fact that the fuel pin model is inherently fine mesh, a relatively coarse mesh discretization of the fuel pin model is nearly equivalent to a fine mesh discretization of the Cartesian Model at least with respect to the precision of the power distribution in the core.

Finally we have studied the effect of using annular boundary conditions in the transport calculation. Here we have compared the thermal flux distribution obtained using the Cartesian model with those obtained using the annular model. The mesh splitting that was selected in both calculations is $n = 2$. The relative differences in the flux distribution along the x axis increases rapidly as one approaches the boundary (see Figure 8). These differences always remain smaller than 1.5 % inside the fuel region and 2.5 % in the reflector. Note that a small part of these differences can be associated with the fact that the annular model generates a finer mesh than that used in the Cartesian model at the reflector/void interface. However, most of these differences can be attributed to the fact that the leakage in the annular model takes place through a surface which is around 25 % smaller than in the Cartesian case.

While the 1/8 core model is useful for convergence studies it does not provide an adequate representation of the CANDU-6 reactor (the number of fuel regions in the core is reduced from 380 to 376). The quarter core model is more appropriate and the convergence studies indicate that a mesh splitting of $n = 2$ for the pin model and $n = 3$ for the Cartesian model is adequate to maintain an upper limit of 2.0 % on the power distribution error in the core.

IV.C. Void Effect

The transport calculations required for the CVR evaluation were performed for the three different transport models with different values for the mesh splitting parameter n. The CVR, computed using Eq. (3), are presented in Table 1.

Table 1: Computed CVR for various transport models

	n	Cooled	Voided	ρ (mk)
Annular k_{eff}	2	1.0235	1.0388	14.4
Cartesian k_{eff}	2	1.0232	1.0385	14.4
Cartesian k_{eff}	3	1.0292	1.0444	14.1
Pin k_{eff}	2	1.0144	1.0301	15.0

The first observation is that contrarily to what is observed in the diffusion calculations, mesh splitting has a relatively large effect on k_{eff} where a difference of 6 mk is observed in the Cartesian case when n is increased from 2 to 3 . For the 1/8 core Cartesian model increases of 6.8 mk and 1.6 mk are observed in k_{eff} when passing from n=2 to 3 and from n=3 to 4 respectively. As a result, a decrease of 0.3 mk in CVR is observed when passing from n=2 to 3 in the Cartesian model. On the other hand, the effect of the boundary conditions on k_{eff} and ρ are weak (< 0.3 mk). The use of a pin instead of a homogeneous fuel model has a 15 mk effect on k_{eff} leading to a difference of up to 0.9 mk in the CVR. This suggests that homogenizing the

moderator with the fuel and coolant region reduces the effect of coolant voiding on the overall cell properties.

V. TRANSPORT-DIFFUSION COMPARISON

For the transport calculations we have selected the $n = 2$ pin model while for the diffusion calculations, the 104×104 Cartesian mesh with cylindrical boundary conditions has been considered.

We first studied the relative effect of voiding on the power distribution obtained using diffusion and transport theory which are presented in Figure 9. The main observation is that voiding flattens the power distribution inside the core. In diffusion, this means a reduction in power of nearly 1 % for the central fuel cells with an increase of up to 2.8 % at the core periphery. In transport this flattening effect is slightly lower. By comparing the CVR from diffusion and transport calculations a difference of 1.3 mk is obtained which corresponds to approximately 10 % of its value. This difference is reduced to 0.4 mk if the Cartesian model (which is in fact similar to the diffusion model) is considered.

Finally a comparison of the diffusion and transport power distributions can be found in Figure 10 for both the cooled and voided cases. Typically, the transport power distribution is flatter than that computed using the diffusion calculations. As expected, the power in the outer fuel rings is under-evaluated in diffusion theory where differences of up to 6.6 % are observed. This automatically leads to an over-estimation of the power in the center of the core. This effect is only slightly reduced when the core is voided.

VI. CONCLUSIONS

After revisiting the various approximations used in diffusion theory we have shown that the cylindrical boundary are the most precise. We also observed that a mesh of 104×104 regions is required to obtain a spatially converged diffusion solution. The boundary conditions and the mesh splitting have no effect on k_{eff} or the CVR.

The main transport approximation we analyzed is the flat source approximation. We observed that the transport solution is spatially converged only when a relatively fine mesh is selected. In fact the homogeneous Cartesian model requires a mesh with 162×162 regions while for the pin model a slightly coarser mesh can be considered (108×108). As in the case of diffusion, refining the mesh has a very small effect on the CVR. However, selecting a pin rather than a homogeneous fuel cell description increases the CVR by nearly 1 mk.

Our results indicate that the power distribution in the outer fuel rings is slightly under estimated in diffusion theory. The voiding effect on power distribution is very similar for both transport and diffusion. A difference of 0.4 mk in the CVR is found between our best diffusion model and the finer Cartesian transport model. This difference increases to 1.3 mk when the coarser pin transport model is considered. Most of this difference can be attributed to the change in homogenization technique when passing to the pin model in transport and to the fact that the spatial mesh in this case is still relatively coarse.

ACKNOWLEDGMENTS

This work was supported in part by a grant from the Natural Sciences and Engineering Research Council of Canada.

REFERENCES

[1] J.V. Donnelly, "WIMS-CRNL: A User's Manual for the Chalk River Version of WIMS", *Atomic Energy of Canada Limited*, Report AECL-8955 (1986).

[2] G. Marleau, A. Hébert and R. Roy, *A User's Guide for DRAGON*, Report IGE-174 Rev. 5, Institut de Génie Nucléaire, École Polytechnique de Montréal (2000).

[3] B. Rouben, "An overview of Current RFSP-Code Capabilities for CANDU Core Analysis", *Atomic Energy of Canada Limited*, Report AECL-11407 (1996).

[4] E. Varin, A. Hébert, R. Roy and J. Koclas, *A User's Guide for DONJON*, Report IGE-208 , Institut de Génie Nucléaire, École Polytechnique de Montréal (2000).

[5] A. Hébert, "Development of a Second Generation SPH Technique for the Pin-by-Pin Homogenization of a Pressurized Water Reactor Assembly in Hexagonal Geometry", *Trans. Am. Nucl. Soc.*, **71**, 253 (1994).

[6] D. Rozon and W. Shen, "A Parametric Study of the DUPIC Fuel Cycle to Reflect Pressurized Water Reactor Fuel Management Strategy" *Nucl. Sci. Eng.*, **138**, 1-25 (2001).

[7] R. Baril and G. Hotte, " Modèle du réacteur pour les calculs HQSIMEX," G2-RT-93-01, Hydro-Québec, 1997.

[8] R. Roy, D. Rozon, A. Hébert and G. Hotte, "Treatment of Circular Boundary Conditions in Neutron Diffusion Calculations", *Third International Conference on Simulation Methods in Nuclear Engineering*, Montréal, Québec, April 18-20, 1990.

[9] A. Hébert, "TRIVAC, A Modular Diffusion Code for Fuel Management and Design Applications", *Nucl. J. of Canada*, **1**, 325 (1987).

[10] K.O. Ott and W.A. Bezella, *Introductory Nuclear Reactor Statics*, American Nuclear Society, La Grange Park (1983).

[11] A. Hébert, "Development of the Nodal Collocation Method for Solving the Neutron Diffusion Equation", *Ann. Nucl. Energy*, **14**, 527-541 (1987).

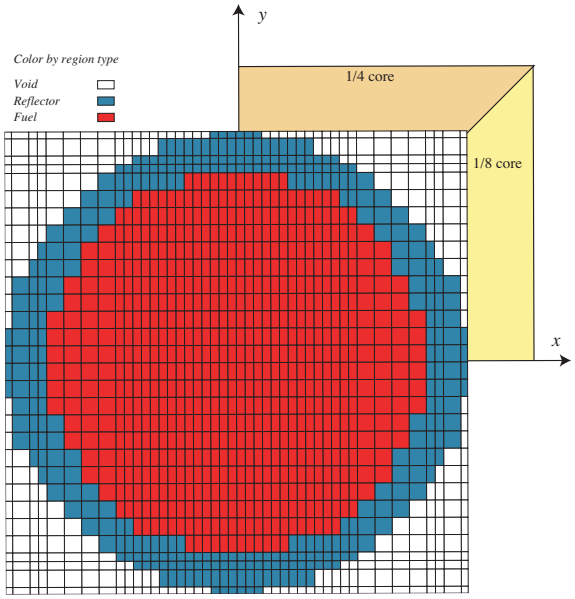

Figure 1: Cartesian 2–D model for the CANDU-6 reactor

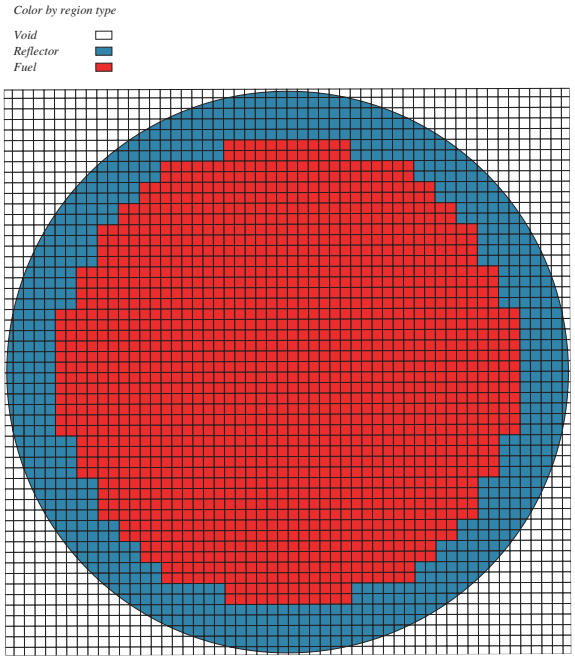

Figure 2: Annular 2–D model for the CANDU-6 reactor

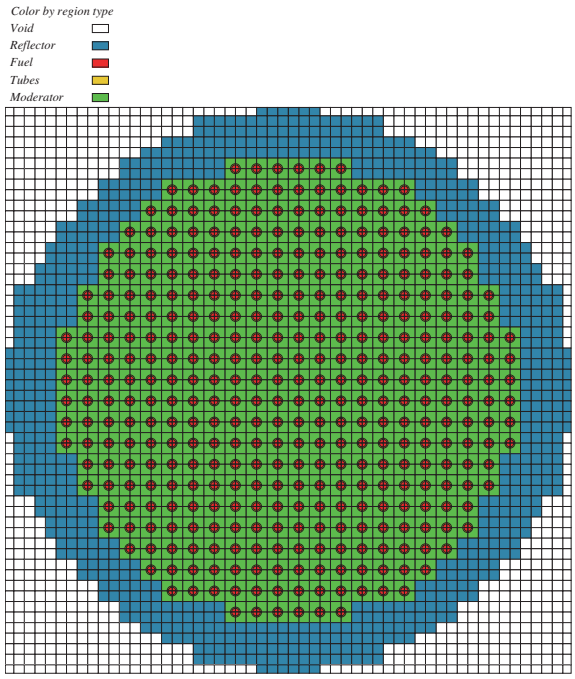

Figure 3: Cartesian 2–D model with fuel pins for the CANDU-6 reactor

	Power Model with cylindrical BC											Relative differences "ZERO" - cylindrical BC										
	12	13	14	15	16	17	18	19	20	21	22	12	13	14	15	16	17	18	19	20	21	22
A	260	231	231									-0.8	-0.9	-2.2								
B	347	315	274	281	236	208						-0.9	-1.0	-1.5	-2.5	-3.8	-5.3					
C	408	421	363	342	298	243	213					-0.2	-0.5	-0.8	-1.2	-2.0	-3.3	-5.2				
D	556	520	466	405	402	351	294	239				0.0	-0.2	-0.2	-0.5	-1.2	-2.0	-3.1	-5.0			
E	653	608	604	541	482	398	344	269	239			0.2	0.0	0.0	-0.2	-0.6	-1.3	-1.7	-3.0	-4.6		
F	788	696	704	608	529	496	431	312	281			0.4	0.4	0.3	0.0	-0.2	-0.4	-0.9	-1.3	-2.5		
G	892	820	803	733	634	549	495	381	322	255		0.6	0.5	0.4	0.4	0.2	0.0	-0.4	-0.8	-1.2	-2.0	
H	970	914	822	809	720	652	558	437	323	281		0.7	0.7	0.6	0.5	0.4	0.3	0.2	-0.2	-0.3	-0.7	
J	972	992	892	854	768	653	570	488	358	285	213	0.7	0.7	0.7	0.6	0.7	0.5	0.4	0.2	0.0	0.0	0.5
K	1069	1026	950	855	842	745	637	507	387	282	236	0.7	0.8	0.7	0.7	0.7	0.5	0.5	0.4	0.5	0.7	0.8
L	1049	998	1014	936	864	730	627	486	424	319	244	0.9	0.8	0.8	0.7	0.6	0.7	0.6	0.6	0.5	0.3	1.6

Figure 4: Power differences between the 44×30 and 54×54 diffusion models.

(Cyli1-Cyli2)/Cyli2*100

	12	13	14	15	16	17	18	19	20	21	22
A	-0.8	-1.3	-2.1								
B	0.3	-0.6	-1,4	-1.1	-2.1	-2.8					
C	-0.5	0.0	-0.3	-0.6	-1.0	-1.6	-3.2				
D	0.4	0.2	-0.2	-0.5	0.0	-0.3	-1.0	-2.8			
E	0.3	0.0	0.5	0.2	0.0	-0.3	-0.6	-1.5	-2.8		
F	0.6	0.0	0.3	0.0	-0.2	0.0	0.0	-1.3	-2.1		
G	0.6	0.2	0.6	0.4	0.0	-0.2	0.0	-0.5	-0.6	-2.7	
H	0.7	0.4	0.1	0.7	0.1	0.5	0.4	-0.2	-0.9	-1.4	
J	0.2	0.6	0.2	0.4	0.1	-0.2	0.0	0.0	-0.6	-1.0	-2.3
K	0.8	0.5	0.3	0.1	0.5	0.5	0.5	0.0	-0.3	-1.1	-0.8
L	0.5	0.2	0.7	0.4	0.6	0.1	0.2	-0.4	0.0	-0.3	-1.2

Figure 5: Power differences in diffusion model with cylindrical boundary conditions for 2 different mesh splitting

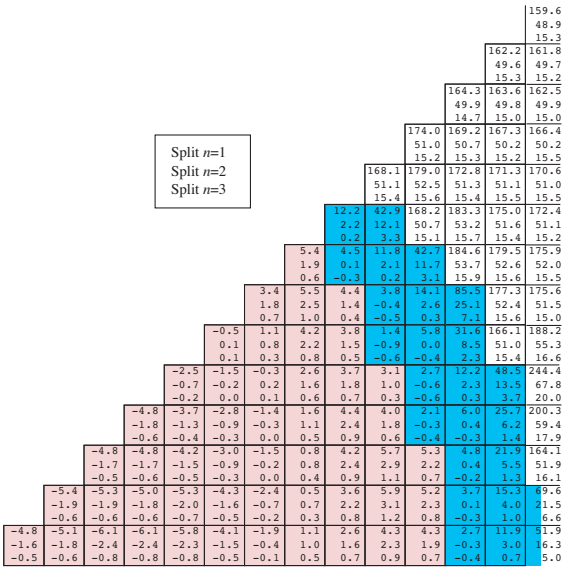

Figure 6: Relative differences in transport flux as a function of split level n. The reference values are for the Cartesian model with $n = 4$.

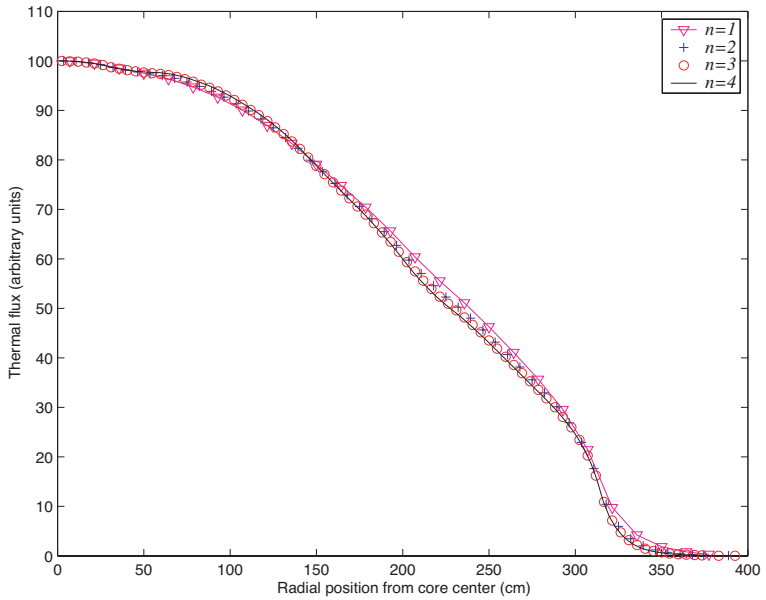

Figure 7: Thermal transport flux along the x axis as a function of split level n.

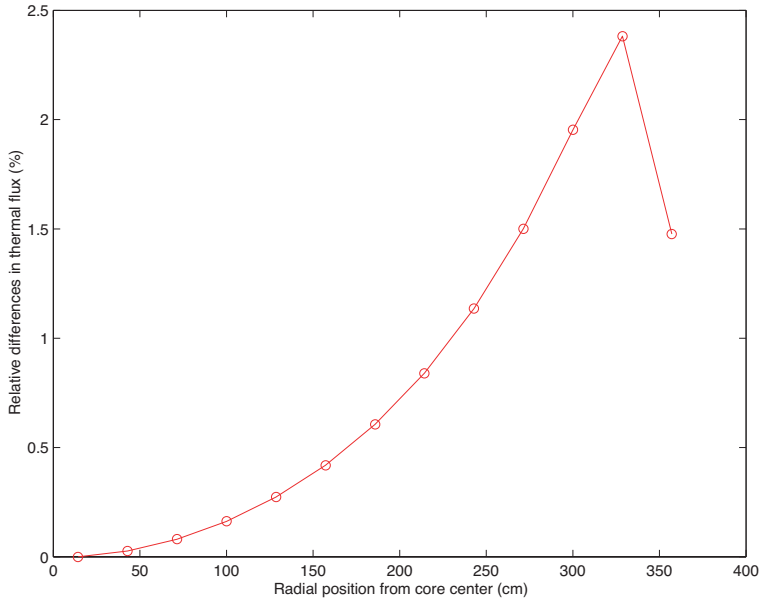

Figure 8: Effect of annular boundaries on the thermal flux distribution along the x axis.

	Diffusion 100*(Voided-Cooled)/Cooled											Transport 100*(Voided-Cooled)/Cooled										
	12	13	14	15	16	17	18	19	20	21	22	12	13	14	15	16	17	18	19	20	21	22
A	2.3	2.1	3.0									1.1	1.3	1.7								
B	1.2	0.9	1.1	2.5	2.5	3.3						0.8	0.3	0.3	1.4	1.2	1.9					
C	0.0	0.2	0.3	0.6	1.0	1.2	2.8					0.0	0.2	0.0	0.3	0.3	0.4	1.4				
D	0.0	0.0	0.0	0.0	0.5	0.9	1.4	2.4				0.0	-0.2	0.0	-0.2	0.2	0.6	1.0	1.2			
E	-0.3	-0.5	0.0	0.0	0.0	0.3	0.3	1.1	3.3			-0.2	-0.2	0.0	-0.2	-0.2	-0.2	0.0	0.4	2.1		
F	-0.1	-0.4	-0.3	-0.5	-0.4	0.2	0.5	0.6	1.7			0.1	-0.4	-0.1	-0.3	-0.4	0.0	0.2	0.0	1.0		
G	-0.5	-0.6	-0.3	-0.3	-0.3	-0.2	0.0	0.5	1.2	2.7		-0.1	-0.3	-0.1	-0.1	-0.3	-0.2	0.0	0.0	0.6	1.5	
H	-0.3	-0.7	-0.7	0.1	-0.4	0.2	0.5	0.2	0.3	2.5		0.1	-0.3	-0.5	0.4	-0.1	0.2	0.4	0.0	0.3	1.4	
J	-0.8	-0.6	-0.8	-0.6	-0.5	-0.5	-0.2	0.2	0.6	1.4	2.8	-0.4	-0.2	-0.5	-0.2	-0.3	-0.3	-0.2	0.0	0.0	0.7	1.3
K	-0.7	-0.8	-0.8	-0.8	-0.5	0.0	0.0	0.0	0.3	0.7	2.1	-0.1	-0.3	-0.4	-0.5	0.0	0.1	0.2	-0.2	0.0	0.3	1.2
L	-0.9	-0.9	-0.6	-0.8	-0.6	-0.5	-0.3	0.0	0.5	0.9	2.4	-0.5	-0.5	-0.1	-0.3	-0.2	-0.3	-0.3	-0.2	0.0	0.3	1.2

Figure 9: Effect of voiding on transport and diffusion power distributions.

	Cooled case 100*(Diffusion-Transport)/Transport											Voided Case 100*(Diffusion-Transport)/Transport										
	12	13	14	15	16	17	18	19	20	21	22	12	13	14	15	16	17	18	19	20	21	22
A	-0.8	-1.7	-0.4									0.4	-0.8	0.8								
B	-2.3	-3.7	-3.8	-1.4	-0.8	1.4						-2.0	-3.0	-3.1	-0.3	0.4	2.8					
C	-2.1	-3.0	-4.2	-4.2	-4.2	-3.1	0.9					-2.1	-3.0	-3.9	-3.9	-3.5	-2.4	2.3				
D	-0.7	-1.9	-2.9	-4.0	-3.6	-3.0	-2.0	2.1				-0.7	-1.7	-2.9	-3.8	-3.3	-2.7	-1.6	3.3			
E	0.8	-0.2	-1.1	-2.4	-3.2	-3.6	-3.4	-2.5	2.5			0.6	-0.5	-1.1	-2.2	-3.0	-3.1	-3.1	-1.8	3.7		
F	2.8	1.2	0.1	-1.0	-2.4	-3.1	-3.1	-4.0	-0.7			2.5	1.2	0.0	-1.1	-2.4	-2.9	-2.9	-3.4	0.0		
G	4.1	2.8	1.7	0.6	-0.8	-1.6	-2.4	-3.8	-3.6	0.4		3.8	2.4	1.5	0.4	-0.8	-1.6	-2.4	-3.3	-3.0	1.5	
H	4.9	3.4	2.1	1.8	0.4	-0.6	-1.6	-3.5	-4.7	-3.1		4.5	3.1	1.9	1.5	0.1	-0.6	-1.4	-3.3	-4.7	-2.0	
J	4.5	3.7	2.4	1.9	0.9	-0.3	-1.6	-3.6	-5.3	-6.2	-4.0	4.1	3.3	2.1	1.6	0.7	-0.5	-1.6	-3.4	-4.7	-5.5	-2.6
K	4.7	4.1	3.0	2.4	2.1	0.8	-1.1	-3.4	-5.6	-6.6	-5.6	4.1	3.6	2.6	2.0	1.6	0.7	-1.2	-3.2	-5.4	-6.2	-4.7
L	4.1	4.0	4.0	3.2	2.5	0.7	-1.6	-3.9	-5.1	-6.2	-5.4	3.7	3.6	3.5	2.8	2.2	0.4	-1.6	-3.8	-4.7	-5.6	-4.2

Figure 10: Comparison of transport and diffusion power distributions for voided and cooled configurations.